Temperature Coefficients of the Rate of Cl Atom Reaction with HBr in the 228−368 K Range at Millitorr Pressures

Otto Dobis and Sidney W. Benson*

Loker Hydrocarbon Research Institute, University of Southern California, University Park, Los Angeles, California 90089-1661

Received: June 11, 1996; In Final Form: November 4, 1996[⊗]

Temperature coefficients for the kinetics of reaction Cl + HBr → HCl(v,j) + Br have been measured in the range 228−368 K using the very low-pressure reactor (VLPR) system. This experimental technique permits measurement of both the reactant consumption and product formation rates under second-order conditions and achieves mass conservation of 98 ± 2% for the overall chemical change in the reactor. Thermalization of vibrationally and rotationally excited HCl product is well attained in this system. A simple Arrhenius function describes the thermal rate constant as $k = (1.99 \pm 0.10) \times 10^{-11} \exp[-(710 \pm 29)/RT]$ cm^3/(molecule s). The measured activation energy is in good agreement with $E_a = 0.72$ kcal/mol obtained from total energy balancing of energy partition among the reaction products, while the A factor indicates a bent configuration of the transition state.

Introduction

The relatively fast and exothermic reaction of

$$\mathrm{Cl} + \mathrm{HBr} \xrightarrow{1} \mathrm{HCl}(v, j) + \mathrm{Br}, \quad \Delta H_0 = -15.7 \text{ kcal/mol}$$

is a prominent representative of the heavy−light−heavy type of elementary hydrogen exchange reaction of atom + diatomic molecules.

In our preceding paper[1] we have shown that our very low-pressure reactor (VLPR) system is well suited for the chemical kinetic investigation of reaction 1 under second-order conditions at 298 K temperature. Mass spectrometric analysis allows us to measure both the reactant consumption and product formation rates, providing therewith an excellent mass balance cross-check. Variations of residence times in the flow cell reactor using different sizes of reactor exit orifices make it possible to identify the existence of any side reactions, such as the wall removal of Cl or Br atoms—which are effectively prevented by the thin Teflon coat of the reactor inner surface—or the back reaction of Br atom with vibrationally excited HCl product. It was also shown that although the relatively long residence time compared to the spontaneous emission decay of all excited species formed ensures a complete thermalization, the collisional quenching alone is also sufficient to reduce HCl(v) to below 1% of the overall HCl concentration.

The knowledge of the well-defined thermal rate constant of reaction 1 has some theoretical and practical significances. It can be used for selecting accurate parameters of the potential energy surface for quasi-classical trajectory (QCT) study[2−4] of exoergic reaction 1. This will give a London−Eyring−Polanyi−Sato (LEPS) surface calibrated with known thermal kinetic data, whereupon the vibrational and rotational energy disposals in the forward reaction 1 can be calculated from detailed balancing and microscopic reversibility.[5]

Since reaction 1 is the pumping stage of a pulsed Cl + HBr chemical laser, the thermal rate constant k_1 is an input parameter, along with initial vibrational and rotational (v, j) distributions, for the laser gain calculation.[6,7]

Equally important is the accurate determination of the temperature coefficients for reaction 1. The translational contribution, $E_a + (3/2)RT$, to the total energy of the reaction system[8] may constitute 9%, and this thermal energy, together with the rotational (RT) contribution, provides the excess energy for $v = 1$, 2 excitations of HCl product. With $E_a \approx 0$, the $v = 2$ excitation of HCl could hardly be achieved.[6] On the other hand, a QCT calculation[2] with dynamic variables not "calibrated" for known thermal kinetic data of reaction 1 results in E_a as high as 1.9 kcal/mol derived from the calculated rate constants at 300 and 1000 K. Consequently, it also gives a high-energy disposal of 58% for the $v = 2$ excitation of HCl product compared to the 20% found by IR chemiluminescence measurement.[8]

Direct experimental studies of the temperature coefficients for reaction 1 are scarce,[9−12] and some of them are controversial.[10,11] Therefore, we have decided to proceed with our VLPR investigation of reaction 1 in the range 228−368 K. The results are presented in the following.

Experimental Section

The VLPR system used for these measurements is the same three-stage, all turbo-pumped system in which the 298 K investigations were carried out.[1]

The thin Teflon-coated, cylindrical reactor cell of volume $V_r = 217.5$ cm^3 has a heating/cooling glass jacket connected to a thermostat bath circulator. At 333 and 368 K, a HAAKE FS2 type circulator was used. It was repleaced at 265 and 228 K by a Neslab ULT-80DD refrigerated bath circulator. Two thermocouples are mounted in the heating/cooling jacket, one at the bottom, the other at the top of the reactor cell, and the circulation speed of the bath fluid is adjusted to eliminate any measurable temperature difference between the two thermocouples. A heat-insulating cover is also applied to the outer surface of the reactor jacket to assist the uniform temperature setting and to avoid ice deposition at low temperatures. Such thermostating keeps the reactor temperature within ±0.1 °C over the entire temperature range.

The reactor cell operates in the Knudsen flow regime. The reactor base is sealed to a Teflon-coated, rapidly adjustable slide mechanism[13] having three interchangeable escape orifices with

[⊗] Abstract published in *Advance ACS Abstracts,* February 1, 1997.

S1089-5639(96)01694-5 CCC: $14.00

TABLE 1: Increase in Br Mass-Signal Intensity Ratio (IR) with Microwave Power in the Cl-Free System[a]

microwave power, W	$\frac{I_{Br}}{I_{Br}+I_{HBr}} \times 10^2$, $V_1 = 20$ V	$\frac{I_{Br}}{I_{Br}+I_{HBr}} \times 10^2$, $V_1 = 40$ V
0	0.23 ± 0.01	25.45 ± 0.04
20	2.49 ± 0.12	27.05 ± 0.22
30	2.30 ± 0.02	27.33 ± 0.07
40	2.63 ± 0.06	27.60 ± 0.18
50	2.76 ± 0.06	28.05 ± 0.10
60	3.14 ± 0.04	27.96 ± 0.02
70	3.09 ± 0.02	27.61 ± 0.15
80	2.95 ± 0.04	28.32 ± 0.07
$\Delta[\overline{IR(W)} - IR(W=0)]_{average}$	2.36 ± 0.29	2.25 ± 0.40

[a] Flow rates used: F(He) = 3.245 × 10^{13} and F(HBr) = 2.69 × 10^{12} molecules/(cm^3 s). T = 333 K, orifice ϕ_3, $\sum P_i$ = 0.31 mTorr.

diameters of 0.193, 0.277, and 0.485 cm. This change in the gas escape rate permits variation of the reactor residence time by a factor of 5 in three steps. The use of these orifice sizes in different experimental runs is indicated as ϕ_2, ϕ_3, and ϕ_5, respectively, in Table 2 and marked with different symbols in Figure 1. With our reactor volume V_r, the first-order escape rate constants for a gas component of mass M are given by $k_{eM} = a_\phi(T/M)^{1/2}$ s^{-1}, where T is the absolute temperature and a_ϕ = 0.258 for ϕ_2, 0.546 for ϕ_3, and 1.321 for ϕ_5 orifices.[13] All escape rate constants appearing in eqs 1, 1a, and 2 were calculated with the above formula at different temperatures. With the reactor surface area of 222 cm^2, depending on the escape orifice size used, wall collisions are generally 10^2-10^3 times more frequent than reactive collisions in the cell.

The VLPR technique delivers an effusive molecular beam through the selected exit orifice, which is chopped by a tuning fork and further collimated by two pinholes at the entrances of two successive differentially pumped chambers to reduce the background mass signals. This beam is sampled with the off-axis mass analyzer of a BALZERS QMG 511 quadrupole mass spectrometer whose mass signal is fed to a phase sensitive lock-in amplifier tuned to the chopping frequency. Mass ranges of kinetic interest are repeatedly scanned, usually 20−25 times to give a good statistical average, and the mass intensities are recorded for data acquisition. Each mass signal is corrected for its small background value recorded prior to start-up of reaction.

Gas inlets are located at the top of the reactor cell for separate inlet flows of Cl_2/He composition and HBr. They are preceded by resistive capillary flow subsystems for regulating the fluxes of initial gas components with the use of Validyne transducers. The flow of a Cl_2/He mixture traverses a phosphoric acid-coated quarz discharge tube centered in the OPTHOS microwave generator cavity of a McCarrol antenna before arriving at the tapered capillary inlet of the reactor cell.

This strictly controlled gas inlet and outlet dynamics establish the well-defined steady-state conditions in the reactor cell. Back-diffusion from the reactor to upstream gases is prevented by the very small conductance of inlet capillaries compared to the conductance of exit apertures. We have never encountered any problem with back-diffusion of gases into the microwave discharge region. Since the study of the H + HBr reaction[14] carried out in an identical VLPR system showed some HBr back-diffusion in conjunction with the observed H atom balance deficiency and small Br_2 formation, which is inversely proportional to the microwave power, we decided to check this problem by running our microwave discharge with pure He flow. The results are summarized in Table 1.

In the first line of Table 1, the data are obtained with concurrent but separated He and HBr flows and the microwave turned off. The HBr fragmentation ratios measured with both 20 and 40 V mass spectrometry are the same, within the error limits, as those we have reported[1] for fragmentations with pure HBr flow variation measurements. But when the microwave on the He flow line is turned on, the Br atom signal ratio jumps up by an average of 2.3% and stays fairly constant with increasing microwave power. We have found that when the microwave discharge is operated with pure He flow, a small but well reproducible H atom signal appears in the mass spectrum at m/e = 1. This signal disappears as soon as the relatively large HBr flow is started up. It indicates that our H_3PO_4-coated discharge tube produces H atoms that then react upon mixing in the reactor with HBr. By use of Cl_2/He flow through the microwave, that H atom content is converted into HCl before arriving at the reactor cell and is included in the measured HCl signal value (see column 2 of Table 2). It also justifies the use of our original HBr fragmentation data[1] measured with pure HBr flow for Br and HBr mass signal corrections.

The mass intensity signal, after corrections for background and fragmentation, is proportional to the steady-state concentration of a given substance in the reactor. This strictly linear proportionality is established by measuring the given mass signal intensity (I_M) as a function of the specific flux F(M) according to the relationship $I_M = \alpha_M F(M)$, where α_M is the mass spectral efficiency for an ion peak of mass M and $F(M)$ = flux/V_r in molecule/(cm^3 s). The steady-state concentration of the gas component of mass M can then be calculated from the relation $[M] = F(M)/k_{eM}$. These formulas are universally applied to convert the measured mass signal intensities into concentrations given in Table 2.

Our mass analyzer is quite sensitive for the HBr specific flux measurement. $\alpha_{HBr} = (8.13 \pm 0.18) \times 10^{-11}$ with 20 V (slightly less than α_{Cl2}) and (2.409 ± 0.024) × 10^{-10} with 40 V mass spectrometry. This permits very accurate concentration measurements with very small fluctuations.

In a typical operation the Cl_2/He flow is started first, using a 4.5% Cl_2/He gas mixture (both are Matheson research-grade gases) and the signal intensities of Cl_2 mass isotopes are repeatedly scanned using 20 V electron energy in the mass range m/e = 70−74 for checking the instrumental reproducibility of mass spectral efficiency α_{Cl2}. Then the microwave generator is turned on and its power is adjusted to 100% dissociation of Cl_2, controlled by observing the disappearance of Cl_2 mass signals. Mass range 35−38 is scanned using 20 V electron energy to record the mass signal intensities of Cl atom isotopes at m/e = 35 and 37 and those of HCl at m/e = 36 and 38. The initial Cl/HCl distribution is obtained from these data (column 2 of Table 2), and the initial Cl concentration is calculated as $[Cl]_0 = 2F(Cl_2)I^o_{Cl}/(I^o_{Cl} + I^o_{HCl})k_{eCl}$ (column 3 of Table 2).

TABLE 2: Initial Concentrations[a] of Cl and the Final Steady-State Concentrations of Reactants and Products Measured in the Experimental Runs

no./ϕ_x	$\frac{I^\circ_{Cl}}{I^\circ_{Cl}+I^\circ_{HCl}}\times 10^2$	$[Cl]_0$	$\frac{I_{Cl}}{I_{Cl}+I_{HCl}}\times 10^2$	[Cl]	$\frac{I_{Br}}{I_{Br}+I_{HBr}}\times 10^2$	[Br]	[HBr]	$\sum P_i$[b]
				$T = 368$ K				
1/ϕ2	44.95	15.96	12.08	4.290	84.50 ± 0.55	17.16	3.17	0.66
2/ϕ2	44.95	15.96	5.98	2.124	72.83 ± 0.09	20.56	7.72	0.69
3/ϕ2	47.39	16.83	3.86	1.371	62.27 ± 0.27	23.29	14.20	0.72
4/ϕ2	49.32	20.73	4.88	2.051	70.60 ± 0.27	28.23	11.83	0.84
5/ϕ2	49.32	20.73	2.85	1.198	59.93 ± 0.55	30.40	20.45	0.88
6/ϕ3	50.80	9.39	23.80	4.401	71.97 ± 0.08	6.88	2.70	0.34
7/ϕ3	50.80	9.39	14.93	2.761	62.25 ± 0.54	9.88	6.03	0.36
8/ϕ3	50.80	9.39	8.76	1.620	49.57 ± 0.45	11.21	11.48	0.39
9/ϕ3	53.15	11.63	8.66	1.895	53.20 ± 0.45	14.05	12.44	0.46
10/ϕ3	53.15	11.63	6.72	1.471	49.62 ± 0.21	15.13	15.46	0.47
11/ϕ5	58.68	4.49	38.70	2.961	43.34 ± 0.45	2.32	3.05	0.16
12/ϕ5	61.81	4.73	30.21	2.311	37.01 ± 0.29	3.46	5.93	0.16
13/ϕ5	61.81	4.73	22.79	1.744	30.93 ± 0.20	4.46	10.03	0.18
14/ϕ5	53.13	4.81	20.82	1.885	32.56 ± 0.24	4.11	8.56	0.20
				$T = 333$ K				
1/ϕ2	51.80	17.25	20.34	6.774	88.81 ± 0.31	16.24	2.06	0.55
2/ϕ2	51.80	17.25	12.43	4.140	83.90 ± 0.61	22.02	4.25	0.58
3/ϕ2	51.74	18.60	8.42	3.026	77.48 ± 0.99	22.48	6.58	0.63
4/ϕ2	51.74	18.60	5.65	2.031	69.53 ± 0.49	24.50	10.80	0.65
5/ϕ3	56.89	9.86	24.92	4.105	70.68 ± 0.71	7.84	3.27	0.29
6/ϕ3	56.89	9.86	19.10	3.312	66.91 ± 0.43	10.17	5.06	0.31
7/ϕ3	56.89	9.86	12.62	2.188	56.40 ± 0.35	11.42	8.88	0.33
8/ϕ3	56.89	9.86	7.41	1.285	43.33 ± 0.07	13.04	17.17	0.36
9/ϕ5	56.98	4.09	34.88	2.402	37.35 ± 0.11	2.34	3.96	0.13
10/ϕ5	56.98	4.09	28.88	2.072	34.34 ± 0.31	3.05	6.03	0.14
11/ϕ5	56.98	4.09	21.18	1.520	27.19 ± 0.36	3.79	10.20	0.15
12/ϕ5	56.98	4.09	19.09	1.370	20.69 ± 0.06	4.08	12.18	0.16
				$T = 265$ K				
1/ϕ2	48.10	20.13	6.25	2.615	70.62 ± 0.95	25.37	10.62	0.59
2/ϕ2	48.10	20.13	3.46	1.448	59.49 ± 0.85	28.03	19.41	0.62
3/ϕ2	45.59	17.62	2.45	0.947	47.62 ± 0.21	24.55	26.79	0.60
4/ϕ3	55.53	12.10	10.07	4.155	68.29 ± 0.83	12.78	5.97	0.31
5/ϕ3	55.53	12.10	4.93	1.074	35.69 ± 0.35	16.62	30.13	0.38
6/ϕ3	55.53	12.10	8.85	1.928	50.42 ± 0.54	15.69	15.53	0.34
7/ϕ3	50.84	15.32	13.98	4.213	68.17 ± 0.95	16.73	7.86	0.42
8/ϕ3	56.36	16.98	7.63	2.299	54.58 ± 0.41	22.42	18.78	0.47
9/ϕ5	54.47	4.91	2237	2.017	29.81 ± 0.28	4.43	10.50	0.15
10/ϕ5	55.09	4.59	32.40	2.698	36.63 ± 0.25	2.84	4.94	0.12
11/ϕ5	55.09	4.59	12.91	1.075	19.00 ± 0.35	5.37	23.05	0.18
				$T = 228$ K				
1/ϕ2	52.71	23.78	14.13	6.374	84.70 ± 0.65	26.74	4.86	0.53
2/ϕ2	61.43	27.71	8.65	3.902	77.61 ± 0.67	36.26	10.69	0.57
3/ϕ2	61.43	27.71	4.92	2.220	66.42 ± 0.53	39.66	20.18	0.60
4/ϕ3	52.54	17.07	21.12	6.861	76.47 ± 0.27	15.42	4.78	0.38
5/ϕ3	64.37	20.91	15.94	5.178	70.00 ± 0.49	23.48	10.13	0.41
6/ϕ3	64.37	20.91	8.71	2.830	55.43 ± 0.97	27.82	22.51	0.45
7/ϕ3	56.53	13.28	20.41	4.794	68.16 ± 0.67	13.22	6.21	0.28
8/ϕ3	58.33	13.70	7.46	1.752	45.46 ± 0.48	20.13	24.31	0.34
9/ϕ3	51.59	5.01	30.14	2.929	35.66 ± 0.46	2.83	5.14	0.12
10/ϕ5	51.59	5.01	14.95	1.453	21.48 ± 0.34	5.61	20.62	0.16
11/ϕ5	51.59	5.01	24.31	2.363	30.32 ± 0.30	3.90	9.02	0.13

[a] All concentrations are in units of 10^{11} particles/cm^3. [b] $\sum P_i$ is the total pressure in mTorr units of the system calculated from steady-state concentrations including HCl and He.

Next, the flow of pure HBr (Matheson 99.8% purity, further purified by trap-to-trap distillation) is started and increased gradually until a sizable decrease of Cl mass signal is achieved. Mass range 35−38 is scanned again, and the new Cl/HCl distribution and the steady-state Cl concentration are calculated (columns 4 and 5 of Table 2, respectively). Afterward, the mass spectrometer is tuned to scan the mass range 79−82 using 20 eV and then 40 eV energy. By correction of these mass signals for the known HBr mass fragmentation ratios[1] of $10^2 I_{79}/(I_{79} + I_{80}) = 0.30 \pm 0.08$ with 20 V and 25.64 ± 0.19 with 40 V electron energy (and the same for 81−82 mass combination), they give the Br/HBr steady-state distribution due to reaction 1. With two isotope compositions (^{79}Br and ^{81}Br) and with two different electron energy measurements, four data points are obtained for the Br/HBr changes in each run. Their average is given in column 6 of Table 2. The steady-state concentration of Br atom can be obtained from the inlet flow rate of HBr, since $[Br] = F(HBr)_0 I_{Br}/(I_{Br} + I_{HBr}) k_{eBr}$ (column 7 of Table 2), while the use of the complementary factor with k_{eHBr} gives the steady-state HBr concentration (column 8 of Table 2).

Mass ranges 114−118 and 158−162 were also checked regularly for possible traces of BrCl and Br_2 side reaction products. No evaluable signal increase of these masses over their background values was ever observed.

Results

The well-controlled inlet and outlet flow of gas components establish the true steady-state condition for all chemical changes in the reactor cell. Hence, all kinetic equations are reduced to algebraic equations. With the knowledge of initial and steady-state concentrations, those equations can be solved for the rate constants of all reactions involved. Mass balance, confirmed from mass spectral analysis of all species consumed and produced, also shows that only one chemical reaction is occurring, namely, reaction 1.

The steady-state condition of Cl atom consumption according to reaction 1 gives the exact kinetic equation

$$\frac{\Delta[\mathrm{Cl}]}{[\mathrm{Cl}]}k_{\mathrm{eCl}} = k_1[\mathrm{HBr}] \tag{1}$$

where $\Delta[\mathrm{Cl}] = [\mathrm{Cl}]_0 - [\mathrm{Cl}]$. Alternatively, the steady-state kinetics of Br atom formation gives

$$\frac{[\mathrm{Br}]}{[\mathrm{Cl}]}k_{\mathrm{eBr}} = k_1[\mathrm{HBr}] \tag{1a}$$

The measured relations between specific fluxes, $F(\mathrm{M})$, and concentrations lead to mass balances between the chemical displacement of all substances in reaction 1:

$$\Delta[\mathrm{Cl}]k_{\mathrm{eCl}} = [\mathrm{Br}]k_{\mathrm{eBr}} = \Delta[\mathrm{HBr}]k_{\mathrm{eHBr}} = -\Delta[\mathrm{HCl}]k_{\mathrm{eHCl}} \tag{2}$$

where Δ represents the difference between the initial and final steady-state concentrations. All measured concentration data for solutions of eqs 1, 1a, and 2 are given in Table 2 directly or can be be derived from these by simple combinations.

The relative Cl atom consumption rates and the alternative Br atom formation rates in different runs at selected temperatures are presented in Figure 1, plotted according to eqs 1 and 1a. Crossed symbols represent the data obtained from Br formation kinetics. The data fit straight lines passing through the origin. This indicates the absence of side reactions including surface reactions. Slopes give the rate contants of reaction 1 directly at each temperature. Their values obtained with linear regression are shown in each figure. The HBr conversion is varied between 19 and 89%, and it is measured on average with 1% accuracy (column 6 of Table 2).

Although the close accommodations of the data of Cl consumption and Br formation kinetics indicate a good mass balance, an overall view can be obtained by plotting the experimental data according to the mass balance restriction eq 2 derived directly from the combination of eqs 1 and 1a. It is done in Figure 2 by taking all relevant data pairs of Table 2. It shows that all measurements, independent of the temperature and residence time (orifice size) used, conform to an excellent mass balance. The slope (0.979 ± 0.011) indicates that our mass recovery is 98%. This is the real power of our improved VLPR system.

The temperature dependence of the measured rate constants is presented as an Arrhenius plot in Figure 3 with filled circles that include the k_1 value at 298 K from our earlier publication.[1] The drawn line is fitted to these data, and it corresponds to the Arrhenius equation

$$k_1 = (1.99 \pm 0.10) \times 10^{-11} \exp[-(710 \pm 29)/RT] \quad \mathrm{cm^3/(molecule\ s)}$$

The precision values of the A factor and the activation energy are both 5%. Such precision is consistent with the very high precision found at each temperature of the rate constants ($\sim$1.5%).

The results of Nicovich and Wine[12] are also shown in Figure 3 (hexagons) after averaging their tabulated room-temperature data as $k_1 = (5.61 \pm 0.15) \times 10^{-12}$ cm^3/(molecule s). The upper line with square symbols represents the results of Mei and Moore.[9,22.]

Discussion

There are four previous temperature coefficient measurements[9−12] for reaction 1 accomplished with different experimental techniques. A comparison shows a small disagreement in the activation energy and about a factor of 1.3−2.0 in the A factor values. Temperature coefficients derived from QCT calculations[2,4] are not independent, since the input parameters for trajectory calculations are adjusted to a selected thermal rate constant measured at 298 K.

A previous attempt[11] to apply the VLPR system to the kinetic investigation of reaction 1 did lead to erroneous results. At that stage of system development, the system variables had not been explored enough to avoid errors (see comments in ref 1). Too narrow a range of HBr concentrations were used, as well as too a short temperature range. The zero activation energy reported[11] is also not consistent with the thermal energy requirement for HCl($v = 2$) product generation. In addition, there is an erroneous estimation of the A factor. The authors[11] have used a 3D rotor together with a 1D rotor, an excess of one degree of rotational freedom and then neglected an even larger and opposite error, namely, the correction for changing standard states (1 atm to 1 mol/L). We correct these mistakes later in this report.

Relative rate measurements[10] in the Cl/(Cl_2)/C_2H_6/HBr multicomponent flow system of about 25 ms contact time lead to $E_a = 0.82 \pm 0.12$ kcal/mol and $A = (4.1 \pm 0.2) \times 10^{-11}$ cm^3/(molecule s) when the parameters of relative temperature coefficients are put on the absolute basis using the known values[15] for the

$$\mathrm{Cl} + \mathrm{C_2H_6} \xrightarrow{2} \mathrm{HCl} + \mathrm{C_2H_5}$$

standard reaction. Rate constant ratios were calculated from the measured relative decreases of HBr and ethane concentrations according to the simplified, approximate equation

$$\frac{k_1}{k_2} \approx \frac{\ln([\mathrm{HBr}]_0/[\mathrm{HBr}])}{\ln([\mathrm{C_2H_6}]_0/[\mathrm{C_2H_6}])} \tag{3}$$

The authors used some excess (not specified) Cl_2 in their system to convert C_2H_5 radicals produced in reaction 2 back to Cl, thus constituting a short chain reaction in conjunction with step 2:

$$\mathrm{C_2H_5} + \mathrm{Cl_2} \xrightarrow{3} \mathrm{C_2H_5Cl} + \mathrm{Cl}$$

However, since the fastest process in the system is reaction 2, most of the Cl formed will be very rapidly reconverted back to C_2H_5. They were aware of some of the other reactions occurring in this system but trusted to the excess Cl_2 to minimize their effect. Unfortunately some of them can reproduce or

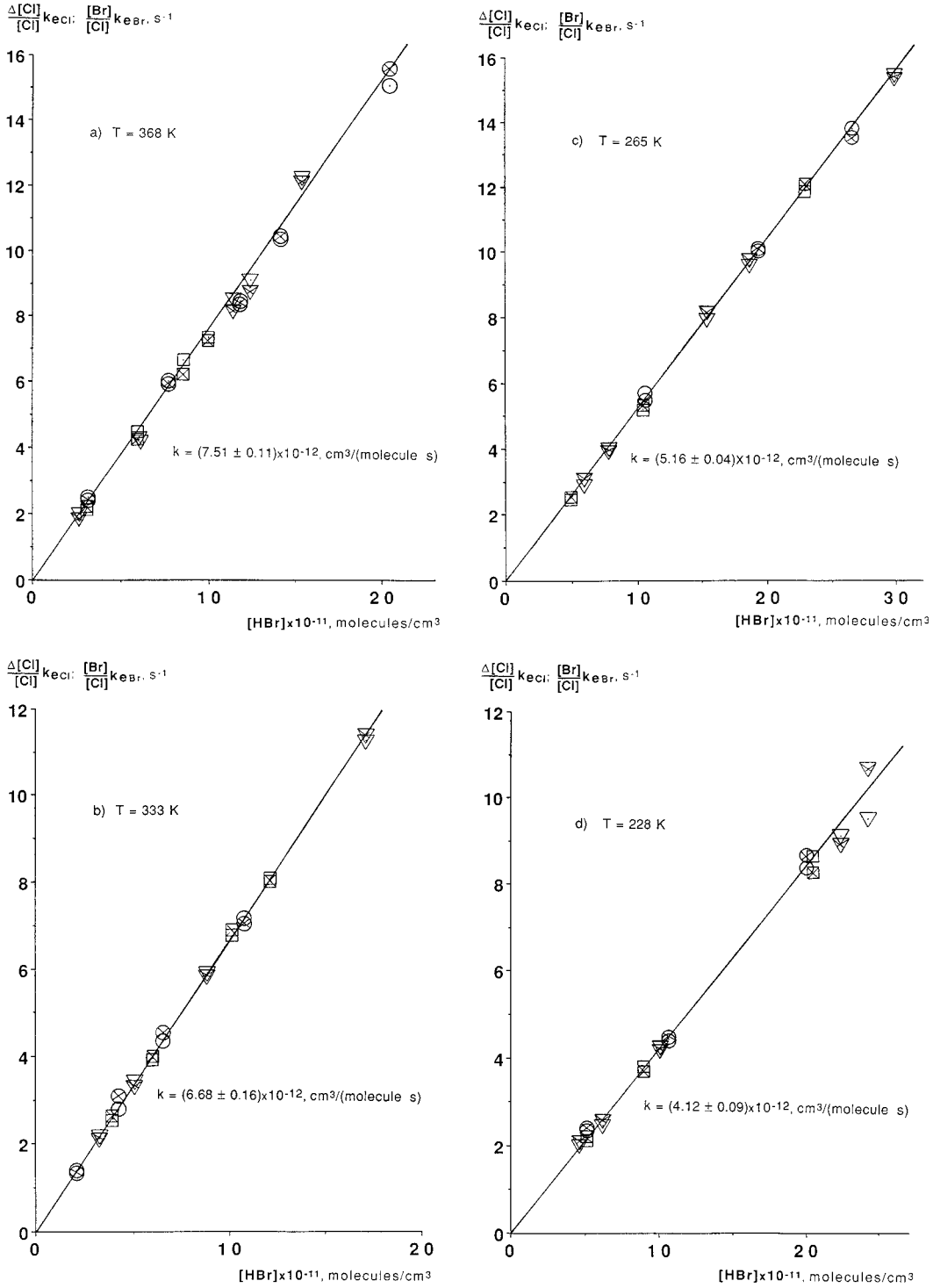

Figure 1. Dependence of relative Cl atom consumption and Br atom formation on the steady-state concentration of HBr according to kinetic eqs 1 (open symbols) and 1a (crossed symbols) at different temperatures. Symbols indicating the orifices used for given data pairs are: dotted circle for $\phi 2$, dotted triangle for $\phi 3$, and dotted square for $\phi 5$.

consume C_2H_6 and or HBr:

$$C_2H_5 + HBr \rightarrow C_2H_6 + Br \quad (4)$$

$$C_2H_5 + Br \rightarrow HBr + C_2H_4 \quad (5)$$

$$2C_2H_5 \rightarrow C_2H_6 + C_2H_4 \quad (6)$$

$$\rightarrow C_4H_{10} \quad (6')$$

Although there is some controversy about the values of the rate constants for reactions 4 and 5 and a further reaction 7,

$$C_2H_5 + Cl \rightarrow C_2H_4 + HCl \quad (7)$$

none of the extreme choices for the various rate constants will justify the use of eq 3 without correction.

We have modeled their system assuming a 50% decomposition of Cl_2 and 50% conversion of Cl to HCl in reaction with the H_3PO_4 wall coating. Using either high values[16] of rate constants for reactions 4, 5, and 7 or low values.[17,18] we find in both cases a quite significant role of these side reactions in the 25 ms reaction time scale of Rubin and Persky's system.[10] We

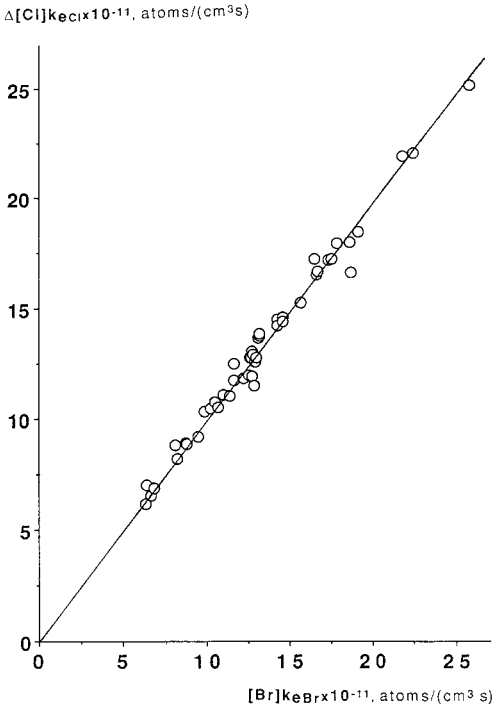

Figure 2. Flow balances between Cl atom consumption and Br atom formation according to eq 2 with all orifices used and at all temperatures of experiments.

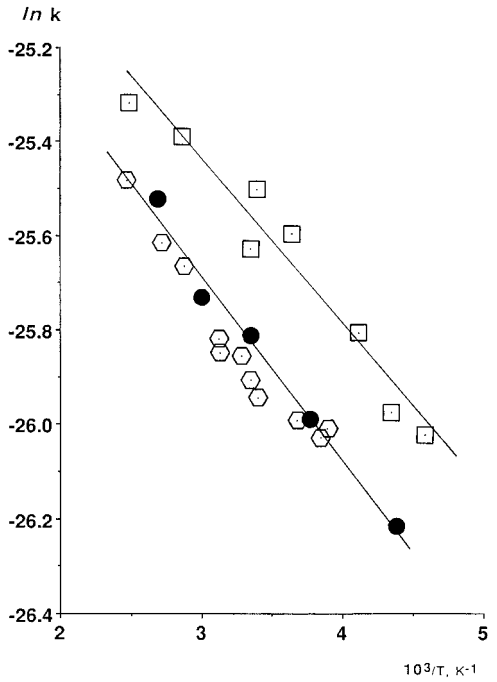

Figure 3. Arrhenius plot of rate constants of reaction 1. Filled circles are present results from Figure 1 and the 298 K data from ref 1 giving the lower line by regression. Hexagons represent the data of ref 12. Upper line and squares show the data of refs 9 and 22.

are further unable to reproduce their high consumption of HBr by factors of 1.4−2.8.

Our earlier study[17a] has shown that the Cl + C_2H_6 reaction system has important side reactions. Its second-order kinetics cannot be described by reducing the entire mechanism to reaction 2. On the other hand, all four side reactions 4−7 have been identified and studied in a similar but less complex Cl/C_2H_6/HBr three-component steady-state kinetic system.[17]

In a recent comment[10a] on our preceding paper,[1] Persky has repeated the arguments presented in the initial paper[10] without, however, offering any additional data to support them, such as modeling the system or considering the important Br + C_2H_5 reaction. We were not given the opportunity to reply to these comments.

The investigation of laser-flash-initiated reaction 1 in the Cl_2/HBr flow system using infrared chemiluminescence (IRCL) from excited HCl formed in the reaction gave a curved Arrhenius relation,[9] concave to the $1/T$ axis. Its form is unusual in that only the high-temperature data (at 402 and 349 K) are responsible for the curvature. Such deviation is usually indicative of a complex mechanism involving two or more concurrent chemical reactions. The authors[9] interpret it instead as a dynamic process coming from attractive attack of Cl on the Br end of HBr followed by rapid bending or tunneling, or both, of the H atom[19] to form the product HCl + Br. They suggested that the direct attack of Cl on the H atom in HBr would have a different rate.

Such an explanation, however, violates the second law. With identical reactants and identical products and thus the same *final* transition state, the result must be independent of the actual dynamic path. From the standpoint of transition state theory (TST), the transition state is in equilibrium with reactants. This equilibrium must be independent of the path to reach it! All possible paths can occur. Some may have consequences for different energy partition in the final products,[20,21] but this type of detail is not within the province of TST. Rather, TST includes *all* conformations and energies of the reactants in the transition state.

By inclusion of the room temperature value of $k_1 = (7.4 \pm 0.7) \times 10^{-12}$ cm^3/(molecule s) measured earlier using the same IRCL technique,[22] the temperature dependent data can be fit to a linear Arrhenius equation in the 402−218 K range with a regular scatter as shown in Figure 3 with square symbols. The line of regression runs nearly parallel with our results, giving $A = (2.54 \pm 0.30) \times 10^{-11}$ cm^3/(molecule s) and $E_a = 0.70 \pm 0.07$ kcal/mol. Although the difference is small, we believe that the 28% higher A factor arises from the use of IRCL signal intensity resolution that does not take into account the HCl($v = 2$) quenching rate and assumes a complete thermalization of rotational states.[22] Since the transition state is of bent configuration (see later), the rotational energy partition is enhanced. As we noted earlier,[1] the IRCL system has no very effective rotational relaxer for the short time scale of its kinetic measurements.

Although the IRCL method extracts k_1 from the HCl* formation rate, the Cl atom resonance fluorescence technique recovers k_1 from the Cl consumption rate measurement following the laser flash initiation of reaction 1 in a similar Cl_2/HBr flow system.[12] As shown in Figure 3, the measured data points marked with hexagons are extremely close to our line in the covered temperature range (maximum deviation of 10%). Averaging the five parallel room-temperature data points, the reported[12] A factor scatter is considerably reduced, giving $A = (2.26 \pm 0.28) \times 10^{-11}$ cm^3/(molecule s) and $E_a = 0.80 \pm 0.08$ kcal/mol. In combination with our data, the Arrhenius parameters would be $A = (2.10 \pm 0.17) \times 10^{-11}$ cm^3/(molecule s) and $E_a = 0.75 \pm 0.05$ kcal/mol.

Our VLPR technique is a steady-state system operating under real second-order kinetic conditions, and we are measuring all the rates of both Cl and HBr consumption, as well as the rates of Br and HCl formation. Equation 2 shows the equality of these rates, which we have demonstrated in Figure 2. It is the most extensive investigation of this apparently simple reaction 1. The measured activation energy also agrees well with $E_a =$

TABLE 3: Structural, Vibrational, and Rotational Parameters for Transition-State Calculation

parameters	Cl	HBr	Cl·H·Br
mass	35.45	80.91	116.36
r(H−Br),[a] Å		1.41	1.71
r(Cl−H),[a] Å			1.58
ν, cm^{-1}		2650	see Table 4
moment of inertia[b] (amu Å^2)			
linear TS		1.979	266.297
		1.979	266.297
		0.0	0.0
bent TS (45°)			227.768
			227.374
			0.394

[a] $r^{\ddagger}$(H·Br) = 1.41 + 0.30 Å and $r^{\ddagger}$(Cl·H) = 1.28 + 0.30 Å. Principal moments of inertia for both the linear and bent transition states were calculated using the GEOM section of the UNIMOL package.[25]

TABLE 4: Transition-State Entropy Calculations for the Cl + HBr Reaction

partial contributors	$\Delta_{298}\, S_p^{\ddagger}$ (linear)	$\Delta_{298}\, S_p^{\ddagger}$ (bent, 45°)
model reaction Cl + HBr → [HBr]‡	−39.49	−39.49
translation	1.08	1.08
electronic	1.38	1.38
rotation	9.74	13.13
vibration[a]		
−(H−Br)$_{2650}$	0.00	0.00
+(H·Br)$_{1150}$ (RC)[b]	0.00	0.00
+(H·Cl)$_{2023}$	0.00	0.00
+2(Cl·H·Br)$_{450}$	1.70	
+(Cl·H·Br)$_{450}$		0.85
totals	−25.59	−23.05

[a] Vibrations of partial bonds are calculated as $\nu^{\ddagger} = 0.7\nu$ cm^{-1}. [b] RC = reaction coordinate asymmetric Br·H·Cl stretch.

0.72 kcal/mol obtained from a total energy balance measured in the reaction products.[23]

The transition state geometry is also an interesting point of potential energy surface calculations for reaction 1. Deviation from a colinear triatomic configuration will deepen the entrance valley interactions,[3] or, alternatively, will increase the potential barrier height.[4] The method of approximating the experimental A factor with the entropy of activation, $\Delta S^{\ddagger}$, estimated with loose or tight transition state geometry,[24] is known as a quick test for geometry.

The HBr reactant was taken for the model standard TS, and the insertion of the Cl atom for the [Cl−H−Br]‡ transition state with either linear or 45° bent structure was made with entropy contributions according to the perturbations and change in the degrees of freedom:[24]

$$\Delta S^{\circ\ddagger} = (S^{\circ}_{\text{model}} - S^{\circ}_{\text{HBr}} - S^{\circ}_{\text{Cl}}) + \sum \Delta S^{\circ}(\text{corrections}) \quad (8)$$

where

$$\sum \Delta S^{\circ}(\text{corrections}) = \Delta S^{\circ}(\text{transl.}) + \Delta S^{\circ}(\text{vib.}) + \Delta S^{\circ}(\text{rot.}) + \Delta S^{\circ}(\text{electronic}) \quad (9)$$

Each term on the right side of eq 9 can be calculated using known thermochemical functions.[26] The input parameters for such calculations are summarized in Table 3, while Table 4 gives the details and summation of the calculated correction terms. The usual uncertainty of such a thermochemically modeled estimation is about 1 eu.

The calculated A factors using the activation entropy values given in the last row of Table 4 are A(linear TS) = 5.07 × 10^{-12} and A(bent TS) = 1.81 × 10^{-11} cm^3/(molecule s). The close agreement of the latter value to the experimental value indicates that the transition state is bent. The observation[21] that the HCl product has a high level of rotational excitation suggests that the separation of products is on a repulsive surface. We may expect rapid relaxation of HCl(j) in our system by the He carrier.

Conclusions

The improved VLPR system is well suited for the investigation of temperature coefficients of reaction 1 in the temperature range 228−368 K. Quick relaxation of vibrationally and rotationally excited HCl product is achieved. This prevents the initiation of HCl(υ, j) side reactions with either Cl or Br atoms, thus providing the ability to make thermal rate constant measurements.

The second-order rate measurement technique permits observation of both the reactant consumption and product formation rates, which gives a mass conservation of 98 ± 2% for the overall chemical change in the VLPR system. This is a powerful check for the absence of any chemical side reactions. At the same time, this technique improves precision and probably the accuracy of rate constant measurements.

Rate constants measured at different temperatures give a normal Arrhenius behavior with $k_1 = (1.99 \pm 0.10) \times 10^{-11}$ exp[−(710 ± 29)/RT] cm^3/(molecule s), where the activation energy well agrees with E_a = 0.72 kcal/mol obtained[23] from total energy balancing of product energy partitions. The A factor value points to a bent transition state configuration. As shown in Figure 3, our temperature dependent measurements are in good agreement with rate constants extracted from the Cl consumption rate measured with time-resolved Cl resonance fluorescence after laser flash initiation of the Cl_2/HBr system.[12] Agreement with time-resolved (IRCL) measurements of the HCl(υ, j) product formation rate[9,22] is somewhat less in part, we believe, because of a slight overestimation of k_1 due to inadequate rotational quenching and some extra IRCL emission from the $\upsilon = 2$ state of HCl product.

Acknowledgment. This work has been supported by a gift from the Occidental Petroleum Co. and a grant from the Petroleum Research Fund administered by the American Chemical Society.

References and Notes

(1) Dobis, O.; Benson, S. W. *J. Phys. Chem.* **1995**, *99*, 4986.
(2) Smith, J. W. M. *Chem. Phys*. **1977**, *20*, 437.
(3) Brown, J. C.; Bass, H. E.; Thompson, D. L. *J. Chem. Phys*. **1977**, *81*, 479.
(4) Broida, M.; Persky, A. *Chem. Phys*. **1989**, *113*, 405.
(5) Levine, R. D.; Bernstein, R. B. *Molecular Dynamics and Chemical Reactivity*; Oxford University Press: New York, 1987; p 177.
(6) Airey, R. J. *J. Chem. Phys*. **1970**, *52*, 156.
(7) Keren, E.; Gerber, R. B.; Ben-Shaul, A. *Chem. Phys*. **1976**, *21*, 1.
(8) Maylotte, D. H.; Polanyi, J. C.; Woodall, K. B. *J. Chem. Phys*. **1972**, *57*, 1547.
(9) Mei, C.-C.; Moore, C. B. *J. Chem. Phys*. **1977**, *67*, 3936.
(10) Rubin, R.; Persky, A. *J. Chem. Phys.* **1983**, *79*, 4310. (a) Persky, A. *J. Phys. Chem*. **1995**, *99*, 16192.
(11) Lamb, J. J.; Kondo, O.; Benson, S. W. *J. Phys. Chem*. **1986**, *90*, 914.
(12) Nicovich, J. M.; Wine, P. H. *Int. J. Chem. Kinet*. **1990**, *22*, 379.
(13) Dobis, O.; Benson, S. W. *Int. J. Chem. Kinet*. **1987**, *19*, 691.
(14) Mitchell, T. J.; Gonzalez, A. C.; Benson, S. W. *J. Phys. Chem.* **1995**, *99*, 6960.
(15) DeMore, W. B.; Sander, S. P.; Golden, D. M.; Hampson, F. R.; Kurylo, M. J.; Howard, G. J.; Ravishankara, A. R.; Kolb, C. E.; Molina, M. J. Chemical Kinetics and Photochemical Data for Use in Stratospheric Modeling. Evaluation No. 11, NASA Panel for Data Evaluation, JPL Publication 94-26; Jet Propulsion Laboratory: Pasadena, CA, 1994; p 25.
(16) Nicovich, J. M.; van Dijk, C. A.; Kreutter, K. D.; Wine, P. H. *J. Phys. Chem*. **1991**, *95*, 9890. Seakins, P. W.; Pilling, M. J.; Niiranen, J. T.; Gutman, D.; Krasnoperov, L. N. *J. Phys. Chem*. **1992**, *96*, 9847. Timonen,

R. S.; Gutman, D. *J. Phys. Chem*. **1986**, *90*, 2987. Kaiser, E. W.; Wallington, T. J.; Andino, J. M. *Chem. Phys. Lett*. **1990**, *168*, 309. Kaiser, E. W.; Rimai, L.; Wallington, T. J. *J. Phys. Chem*. **1989**, *93*, 4094. Mariq, M. M.; Szente, J. J. *J. Phys. Chem*. **1993**, *97*, 7970. Seakins, P. W.; Woodbrige, E. L.; Leone, S. R. *J. Phys. Chem*. **1993**, *97*, 5633.

(17) Dobis, O.; Benson, S. W. *J. Am. Chem. Soc*. **1995**, *117*, 8171.

(18) (a) Dobis, O.; Benson, S. W. *J. Am. Chem. Soc*. **1991**, *113*, 6377. (b) Goldfinger, P.; Huybrechts, G.; Martens, G.; Meyers, L.; Olbregts, J. *Trans. Faraday Soc*. **1965**, *61*, 1933.

(19) Mei, C.-C.; Moore, C. B. *J. Chem. Phys*. **1979**, *70*, 1759.

(20) Nazar, M. A.; Polanyi, J. C.; Skrlac, W. J. *Chem. Phys. Lett*. **1974**, *29*, 473.

(21) Kuntz, P. J.; Nemeth, E. M.; Polanyi, J. C.; Yung, C. E. *J. Chem. Phys*. **1966**, *44*, 1168.

(22) Bergman, K.; Moore, C. B. *J. Chem. Phys*. **1975**, *63*, 643.

(23) Douglas, D. J.; Polanyi, J. C.; Sloan, J. J. *Chem. Phys*. **1976**, *13*, 15.

(24) Benson, S. W. *Thermochemical Kinetics*, 2nd ed.; Wiley: New York, 1976; p 151.

(25) Gilbert, R. G.; Smith, S. C.; Jordan, M. J. T. *UNIMOL: A Program for Calculation of Rate Coefficients for Unimolecular and Recombination Reactions*; Department of Theoretical Chemistry, University of Sydney: Sydney, Australia, 1990.

(26) Thermochemical functions for the calculation of terms of $\sum\Delta S^0$(corrections) are taken from ref 24. They are, at 298 K;

$$\Delta S^0(\text{trans.}) = (2/3)R \ln(\text{M}^{\ddagger}/\text{M}_{\text{model}})$$

$$\Delta S^0(\text{vib.}) = S^{\ddagger}(\text{vib.}) - S^0(\text{vib.})_{\text{model}}$$

$$\Delta S^0(\text{rot.}) = R \ln(I^{\ddagger}\sigma_{\text{model}}/I\sigma^{\ddagger}_{\text{model}})$$

for linear configuration, and

$$\Delta S^0(\text{rot.}) = [11.59 + (R/2)\ln(I^{\ddagger}_{a}I^{\ddagger}_{b}I^{\ddagger}_{c}/\sigma^{\ddagger 2})] - [6.97 + R \ln(I_{\text{model}}/\sigma_{\text{model}})]$$

for bent configuration.

$$\Delta S^0(\text{electronic}) = R \ln[(2S + 1)^{\ddagger}/(2S + 1)_{\text{model}}]$$

$$\Delta S^{\ddagger}_{c} = \Delta S^{\ddagger}_{p} + \Delta nR \ln(eR'T) = \Delta S^{\ddagger}_{p} + 8.35$$

$$A = (ekT/h)\ln(\Delta S^{\ddagger}_{c}/R) = 2.81 \times 10^{-8} \ln(\Delta S^{\ddagger}/R)\ \text{cm}^3/(\text{molecule s}).$$